Solving the puzzle of discrepant variability on monthly time scales implied by SDSS and CRTS datasets

Krzysztof Suberlak,[1]* Željko Ivezić, [1] Chelsea L. MacLeod,[2] Matthew Graham,[3] Branimir Sesar[4]

[1] *Department of Astronomy, University of Washington, Seattle, WA, United States*
[2] *Institute for Astronomy, University of Edinburgh, Royal Observatory, Edinburgh, United Kingdom*
[3] *Center for Data-Driven Discovery, California Institute of Technology, Pasadena, CA, United States*
[4] *National Optical Astronomy Observatory, Tucson, AZ, United States.*

ABSTRACT

We present improved error analysis for the 7,100 CRTS (Catalina Real-Time Transient Survey) optical light curves for quasars from the Sloan Digital Sky Survey Stripe 82 catalog. SDSS imaging survey has provided a time-resolved photometric dataset which greatly improved our understanding of the quasar optical continuum variability: data for monthly and longer timescales are consistent with a damped random walk. Recently, newer data obtained by CRTS provided puzzling evidence for enhanced variability, compared to SDSS results, on monthly time scales. Quantitatively, SDSS results predict about 0.06 mag root-mean-square variability for timescales below 50 days, while CRTS data show about a factor of two larger rms for spectroscopically confirmed SDSS quasars. Our analysis presented here has successfully resolved this discrepancy as due to slightly underestimated photometric uncertainties provided by the CRTS image processing pipelines. The photometric error correction factors, derived from detailed analysis of non-variable SDSS standard stars that were re-observed by CRTS, are about 20-30%, and result in a quasar variability behavior implied by the CRTS data that is fully consistent with earlier SDSS results.

1 INTRODUCTION

Variability can be used to both characterize and select quasars in sky surveys (for a recent overview, see Lawrence (2016)) . Although various time scales of variability can be linked to physical parameters, such as accretion disk viscosity, or corona geometry (Kelly et al. (2011), Graham+2014), the physical mechanism remains elusive, and most viable explanations include accretion disk instabilities (Kawaguchi et al. 1998), surface thermal fluctuations from magnetic field turbulence (Kelly et al. 2009), coronal x-ray heating (Kelly et al. 2011) (see Kozłowski (2016) for review). The diversity of physical scenarios available to explain the origin of quasar variability results in a variety of ways to characterize it. The two most widely used approaches to describe variability of quasars are damped random walk (DRW) and structure function (SF). The DRW model is more suited for light curves with a typical cadence of days (Zu et al. 2013; Kozłowski 2016), whereas an ensemble SF analysis is better for sparsely sampled light curves (Hawkins 2002; Vanden Berk et al. 2004; de Vries et al. 2005; Schmidt et al. 2010; Graham et al. 2014), or review in Kozłowski (2016)). For CRTS sparsely sampled light curves we prefer the SF approach, as more robust than fitting for DRW parameters.

Although SF can be defined in a variety of ways, it can be characterized by a simple broken power law (Schmidt et al. 2010). At short timescales, the variability amplitude increases, following a steeper power law index, until the power law index starts to flatten above the characteristic timescale τ. This knee in the power law description may correspond to a transition from the stochastic thermal process driving the variability, to the physical response of the disk that successfully dampens the amplitude on longer timescales (Lawrence (2016); Kelly et al. (2007); Kelly et al. (2009); Kelly et al. (2011); Collier & Peterson (2001) , (linking the amplitude to the black hole mass)). Indeed, in x-rays quasars are described by a broken power law, where the break timescale is linked to the size of x-ray emitting region (Kelly et al. (2011) in Graham et al. (2014)).

Altough previous studies found that $\tau > 100$ days (MacLeod et al. (2010), Kozłowski (2016)), recently, Graham et al. (2014) used the SF, DRW, and Slepian Wavelet Variance (SWV) analysis for CRTS and SDSS S82 lightcurves. Using SWV on CRTS data they found characteristic time scales at QSO rest frame of $\log_2(\tau) = 5.75$) 54 days, and $(\log_2(\tau) = 8.2)$ - 294 days. Additionally, using this method on S82 data they found a peak at $\log_2(\tau) = 7.25$, and for OGLE at $\log_2(\tau) > 6$. The short timescale of $\tau = 54$ days is surprising, as it is shorter by a factor of two than any previous estimates (MacLeod et al. 2011; Zu et al. 2013).

We set out to reanalyze the CRTS data, and investigate the plausibility of these discrepant timescales.

2   DATA SETS

We study stars and quasars from Stripe 82 (S82), using the Sloan Digital Sky Survey and the Catalina Real-time Transient Survey data. S82 is a large (over 100 deg^2), repeatedly observed reqion of the equatorial sky ($22^h24^m <$ RA $< 04^h08^m$ and |Dec| $< 1.27 deg$) (Sesar et al. 2007; Süveges et al. 2012).

### 2.1   Sloan Digital Sky Survey (SDSS)

We use the SDSS catalog data with robust, five-band near-simultaneous photometry for 9258 quasars, and 1006849 standard stars - we use it for photometric color information and sample selection. The quasar catalog [1] contains spectroscopically confirmed quasars from the SDSS Data Release 7 (Abazajian et al. 2009), based on the SDSS Quasar Catalog IV (Schneider et al. (2008) VizieR Online Data Catalog, 7252, 0), and was compiled by MacLeod et al. (2011) . The standard stars catalog[2] ver. 2.6 was compiled by Ivezić et al. (2007).

2.2   Catalina Real-time Transient Survey (CRTS)

The CRTS data consists of white light (no filter) lightcurves - it was designed to find near-Earth objects, hence short intra-night cadence, to allow a rapid follow up (Graham et al. 2015) . Three survey telescopes (0.7m Catalina Sky Survey Schmidt in Arizona, 1.5m Mount Lemmon Survey telescope in Arizona, and the 0.5m Siding Spring Survey Schmidt in Australia) were equipped with identical, 4kx4k CCDs taking 4 exposures each night (see Djorgovski et al. (2011) for technical details). Although in principle white light magnitudes can be calibrated to Johnson V-band zero point (Drake et al. 2013), we found this step redundant in our analysis.

In this study we used a sample of 7932 spectroscopically confirmed S82 quasars, prepared by B. Sesar, from the Data Release 2, based on the list by MacLeod et al. (2011). The majority (96%) of CRTS quasar lightcurves span the time of 7-9 years, with a mean sampling of 1 to 4 times per night, on 70 nights on average (see Fig.1, upper-left panel). Mean interval between epochs is 209 days (2.2 bottom-right panel), and the mean quasar magnitude is 19.5 mag.

For comparison we use the CRTS lightcurves of 52133 randomly chosen 10% of the S82 standard stars catalog ver.2.6 (Ivezić et al. 2007), extracted by B. Sesar from the CRTS Data Release 2.
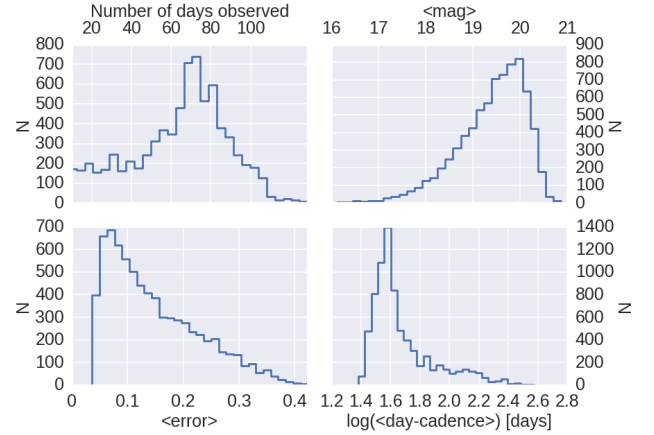
Figure 1. The properties of 7601 day-averaged quasar lightcurves (error weighted mean magnitude, see eq. 1). The upper-left panel shows the distribution of the number of days quasars were observed (that corresponds to the number of day-averaged epochs). The upper-right panel shows the average light curve magnitude. The bottom-left panel shows the light curve averaged error. The bottom-right panel shows the average number of days between epochs. Within that sample , 96% observations of quasars span the time of 7-9 years. 91.2% of quasars were observed between 1 to 4 times per night. We use only quasars with light curve averaged error smaller than 0.3, leaving 7108 quasars in the sample.

2.3   Catalog Matching

To enrich the information about each CRTS object with SDSS color information, we matched positionally the CRTS data to the SDSS data within the S82 using astropy (Astropy Collaboration et al. 2013) `match_to_catalog_sky` routine[3]. Since the SDSS catalog has over 10 times more stars than CRTS, we found an SDSS counterpart to all CRTS stars within 0.01 arcsec matching radius. The SDSS S82 quasar catalog is not significantly larger than CRTS catalog, and for 7586 CRTS quasars we found an SDSS counterpart within 0.36 arcsec. We ignored 15 CRTS quasars for which no SDSS counterpart was found within 1 arcsec.

2.4   Preprocessing

It is common to bin the data to reduce noise, by averaging over timescales shorter than what is required by the science goals. In this study, the hourly timescale of intra-night variability of CRTS lightcurves, with ≈ 4 epochs each night, is much shorter than the timescales of interest on the order of tens of days. Thus, as part of preprocessing we day-averaged all CRTS light curves, following a procedure similar to Charisi et al. (2016), replacing the magnitudes from the j-th night by their mean weighted by the inverse square of error:

$$m_j = \langle m_{ij} \rangle = \frac{\sum_{i=1}^{N} w_{i,j} m_{i,j}}{\sum_{i=1}^{N} w_{i,j}} \tag{1}$$

where $i = 1...N$, is the number of observations per night, with weights $w_{i,j} = e_{i,j}^{-2}$. We estimate the error on the weighted mean by the inverse square of the sum of weights:

$$\sigma_j(m_j) = \frac{1}{\sqrt{\sum_i w_{i,j}}} \tag{2}$$

Finally, to avoid unphysically small errors, we added in quadrature 0.01 mag to σ_j if $\sigma_j < 0.02$ mag.

2.5 Selection

We selected both quasars and stars using a combination of information from SDSS and CRTS. To find magnitude difference between different days we first required that the raw lightcurve has more than 10 epochs, which from initial 52131 stars and 7932 quasars left 49385 stars and 7707 quasars. We thus also removed those lightcurves with less than 10 days of observations, leaving 7601 quasars and 48250 stars. We also required that the lightcurve-average of day-error ($\langle \sigma_j(m_j)\rangle$) be less than 0.3 mag (see Fig.2.2). Since the raw distribution of errors peaks at lower values (mean of 0.19 mag for stars and 0.22 mag for quasars) than the distribution of the weighted mean errors (mean of 0.13 mag for stars and 0.15 mag for quasars), this cut only removes less than 10% of lightcurves. Our final sample consists of 7108 quasars and 42864 stars.

3 ANALYSIS METHODS

To analyze the quasar and stellar lightcurves we consider a relationship between measured data m_j at times t_j, and its "copy" shifted by Δt (Kozłowski 2016). We bin the data in bins of Δt, and calculate statistics that characterize the variability of stars and quasars. Splitting our sample of stars by color into "blue" and "red" we compare their variability properties to those of quasars in three magnitude bins.

3.1 Structure Function

The structure function is a well-studied approach to characterizing lightcurves (Vanden Berk et al. 2004; de Vries et al. 2005; Kozłowski 2016; Graham et al. 2013) . To avoid the uncertain redshift estimate based on SDSS spectra that would be required to correct to the rest-frame variability, we use the observed frame time lags (see Schmidt et al. (2010); Kozłowski (2016)). The magnitude difference $\Delta m_{j,k} = m_j - m_k$ for $\Delta t_{j,k} = |t_j - t_k|$, and the errors added in quadrature : $\sigma_{j,k}^2 = \sigma_j^2 + \sigma_k^2$.

To study the statistical distribution of time-lag magnitude differences in an ensemble of quasars or stars we bin the data in bins of $\Delta t_{j,k}$, or for brevity Δt. For each object we prepared 'master' files containing $\Delta m_{j,k}$, Δt, $\sigma_{j,k}$. Even after day-averaging, with a median lightcurve length of 70 days, each object contributes on average $\sum_{i=2}^{70}(i-1) = 2415$ $\Delta m_{j,k}$ points . Thus we have sufficient amount of pairwise time differences to study their statistical properties by splitting them into 200 linearly spaced bins of Δt. Bin number does not affect significantly the shape of the structure function, and 200 bins is a good choice to provide good time resolution with a large number of $\Delta m_{j,k}$ in each bin.

With various theoretical definitions of structure function (see Kozłowski (2016) for overview), we adopt a view from Ivezić et al. (2014), that SF corresponds to the intrinsic width of the $\delta m_{j,k}$ distribution $\mathcal{N}(\sigma, \mu)$. Each $\Delta m_{j,k}$ has an error, assumed to be drawn from the Gaussian distribution with a known width e_i. Thus each $\Delta m_{j,k}$ (called x_i for brevity, as in Ivezić et al. (2014)), is drawn from a distribution with a total width $\sigma_{tot} = \sqrt{\sigma^2 + e_i^2}$.

Then the likelihood for a set of measurements $\{x_i\}$ is given by a product of likelihoods for each value of x_i:

$$p(\{x_i\}|\mu, \sigma, I) = \prod_{i=1}^{N} \frac{1}{\sqrt{2\pi}\sigma_{tot}} \exp\left(\frac{-(x_i - \mu)^2}{2\sigma_{tot}^2}\right) \tag{3}$$

Using uniform priors, the logarithm of the posterior pdf is :

$$L_p = const - \frac{1}{2}\sum_{i=1}^{N}\left(\ln(\sigma_{tot}^2) + \frac{(x_i - \mu)^2}{\sigma_{tot}}\right) \tag{4}$$

To find $SF = (\sigma)$, we evaluate L_p on a grid of μ, σ, and marginalize over μ to find likelihood for σ:

$$p(\sigma|\{x_i\}, I) = \int_0^\infty p(\mu, \sigma|\{x_i\}, I)d\mu \tag{5}$$

The zero point of the first derivative of this likelihood: σ_0, is the most likely value of σ. An alternative way is to find the 2D maximum of $\exp(L_p)$ to obtain simultaneously both μ_0 and σ_0.

Unfortunately, without any prior constraint on the value of μ_0 or σ_0 this procedure can be computationally expensive. Thus we first find approximate values of σ_0 and μ_0. The sample median is a good estimator of μ_0, and σ_0 can be estimated by:

$$\sigma_0^2 = \zeta^2 \sigma_G^2 - e_{50}^2 \tag{6}$$

where:

$$\zeta = median(\tilde{\sigma}_i)/mean(\tilde{\sigma}_i), \tag{7}$$

$$\tilde{\sigma}_i = (\sigma_G^2 + e_i^2 - e_{50}^2)^{1/2}, \tag{8}$$

$$\sigma_G = 0.741(Z_{75\%} - Z_{25\%}), \tag{9}$$

where Z is the sorted $\Delta m_{j,k}$ per bin, and $e_{50} = median(\sigma_{j,k})$.

Now, if errors were all equal ($e_i = e$), then $e_{50} = e$, and $\tilde{\sigma}_i = \sigma_G$, so that $\zeta = 1$, and thus $\sigma_0^2 = \sigma_G^2 - e^2$.

If errors were not all equal, but very small compared to σ_G, then $\tilde{\sigma}_i \to \sigma_G$, and $\zeta \to 1$, so that $\sigma_0^2 = \sigma_G^2 - e_{50}^2$, but since $e_{50} \ll \sigma_G$, $\sigma_0^2 \approx \sigma_G^2$. This explains why σ_G can be seen as an approximation of SF (see eq.10 in Kozłowski (2016)).

Therefore, to find the best estimate of $SF = \sigma_0$, we evaluate 1000 boostrapped resamples of $\Delta m_{j,k}$ in each Δt bin, and thus find upper and lower limits on the approximate value of σ_0. We use these values as limits on our grid of μ, σ, on which we evaluate the full solution from L_p.

Table 1. Count of stars and quasars, selected by their SDSS r-magnitude. For all objects we also required that the CRTS lightcurve error is smaller than 0.3 mag.

r-mag	red stars	blue stars	quasars
17-18	2993	2795	185
18-18.5	2087	1400	333
18.5-19	1496	2327	747

3.2 Statistics, sample construction

As described above, σ, σ_G and μ are all related in describing the structure function and variability of quasars, and thus we plot them as a function of Δt on Fig.2. As a guide to the width of the $\Delta m_{j,k}$ distribution, we also plot its standard deviation, i.e. the square root of the average of the squared deviations from the mean:

$$\sigma_{stdev} = \sqrt{\frac{\sum(\Delta m_{j,k} - \overline{\Delta m_{j,k}})^2)}{N_{bin}}} \tag{10}$$

To consider the effect of stellar color on variability we divided the sample of stars into two SDSS g-i color bins: "red" stars with $1 < g - i < 3$, and "blue" stars with $-1 < g - i < 1$. We expect blue stars to be preferentially brighter, and have smaller variability than the red stars. See Table 1 for the number of stars and quasars in each color-magnitude bin.

To consider any magnitude-dependent trends in the data, such as increasing photometric error for fainter objects, we split our sample into three magnitude bins: bright 17-18, medium 18-18.5 , and faint 18.5-19 mag. We used SDSS r-magnitude to select the magnitude of objects, which is correlated to the CRTS white light magnitude for both stars and quasars. Table 1 shows the number of objects per magnitude bin.

4   RESULTS

The measured level of variability for standard stars is above the acceptable 0.05 mag rms, and is incompatible with their known non-variability. Fig.2 illustrates the problem, using the four statistics calculated for the 18.5-19 mag bin, as described in Sec. 3.2. Especially SF shows that even on short timescales, stars exhibit a non-zero variability for stars. Based on the SDSS data concerning the same stars, we would expect their SF to be below the level of noise : 0.05 mag (Ivezić et al. 2007). This larger than expected variability is inspected in more detail in Fig.4.

We derive correction factors for CRTS photometric errors using blue stars, since they have similar colors to quasars. Consider the robust with of χ distribution:

$$\chi_i = \frac{\Delta m_i - \overline{\Delta m_i}}{\sigma_i} \tag{11}$$

for pairwise magnitude difference points, but since our lightcurves are symmetric around 0, $\overline{\Delta m_i} \approx 0$. It is worth noting that χ_i is related to chi-square:

$$\chi^2 = \sum_{i=1}^{N} \chi_i^2 \tag{12}$$
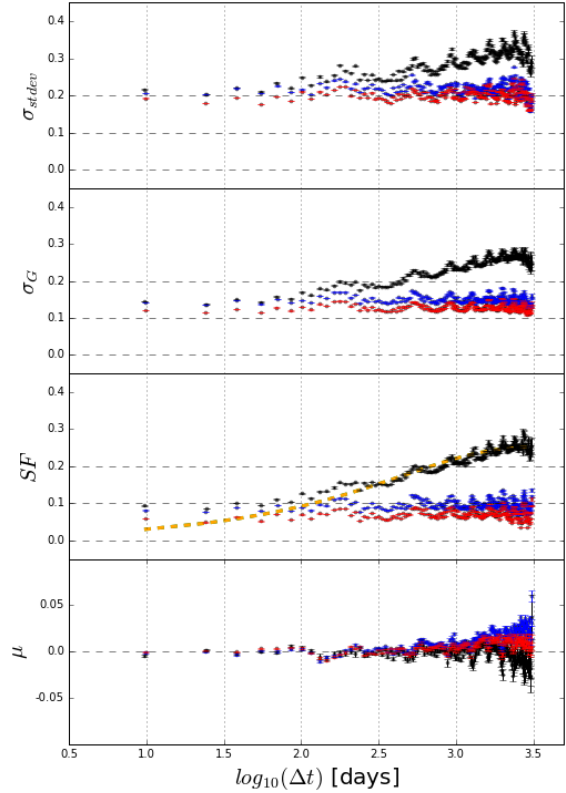
Figure 2. The four panels show statistics calculated for the subsample of 333 CRTS quasars (black points), 1400 "blue" stars (blue points), and 2087 "red" stars (red points), all chosen according to the SDSS r magnitude 18.5 < m < 19. Red and blue stars have $1 < g - i < 3$ and $-1 < g - i < 1$ respectively. All pairwise brightness differences in white light ($\Delta m_{i,j}$) are binned in 200 linearly spaced bins of $\Delta t_{i,j}$. For each bin, we calculate different statistics, from top to bottom panels: the standard deviation σ_{stdev}, the robust Gaussian deviation based on the interquartile range σ_G, the structure function SF, and the mean value of $\Delta m_{i,j}$ per bin:μ. Both μ and σ are found from the 2D maximum of the log-likelihood L_p on the [μ, σ] grid (see eq. 4, and Ivezic+2004). Yellow dashed line on the third panel traces the fiducial Damped Random Walk model. Note how the level of variability for both blue and red stars does not increase with timescale (staying on 0.1 mag level), unlike quasars. Since the variability of stars corresponds here to the measurement noise, until quasars raise above the stellar structure function level (at $\log(\Delta t) > 2$), no claim can be made about their intrinsic variability. Thus any departure of CRTS quasar structure function at low timescales ($\log \tau < 1.7$), is due to incorrect errors (underestimated measurement noise).

Therefore, if σ_i describes well the underlying (Gaussian) error, then in case of no intrinsic variability we would expect $\sigma_G(\chi) = 1$, such as is the case for blue standard stars.

We binned the time lag - magnitude difference points into four $\log(\Delta t)$ bins : one for short timescales $\log(\Delta t) < 1.7$ ($\Delta t < 50$ days), and three for longer timescales : $2.3 < \log(\Delta t) < 2.5$, $2.8 < \log(\Delta t) < 3.0$, and $3.2 < \log(\Delta t) < 3.4$.

Table 2. The correction coefficients, as evaluated based on $\sigma_G(\chi)$ for blue stars.

correction	mag
0.08326	17 - 18
1.04461	18 - 18.5
1.22914	18.5 - 19

We also split the sample in three magnitude bins, which together results in 12 separate $\log(\Delta t)$ - magnitude bins for blue stars and quasars. This allows to check whether there is any dependence of error correction on magnitude or timescale. For each bin we evaluate the histogram of a quantity χ. As shown on Fig.4, the width of χ distribution differs from 1 for blue stars, which means that σ_i is either over or underestimated. Furthermore, at short timescales ($\log(\Delta t) < 1.7$) quasars are indistinguishable from stars in χ. However, at longer timescales quasars show distinct signature of variability - the distribution of χ is much wider for quasars than for stars. To correct the discrepant robust width of stellar χ, we find the correction factor based on the $\sigma_G(\chi_{blue})$. We find that for blue stars there is a magnitude-dependent linear relationship between the robust width of χ distribution, and the $\log(\Delta t)$, but the $\log(\Delta t)$ dependence is an order of magnitude smaller than the magnitude dependence. Therefore we average the value of $\sigma_G(\chi_{blue})$ over all timescales for each magnitude bin, resulting in a single value of correction factor, f_c, per magnitude bin (see Table 2).

Multiplying σ_i by the corresponding f_c brings $\sigma_G(\chi_{Blue})$ to 1, as expected. We thus correct the day-averaged errors, which brings down the variability (see Fig.4):

$$\sigma_{i,corr} = f_c\,\sigma_i \tag{13}$$

As we show in Appendix A, it also is a multiplicative constant that can be applied to correct the raw photometric errors:

$$e_{corr} = f_c\,e \tag{14}$$

5 CONCLUSIONS

We analyzed the error properties of the CRTS sample of quasars and standard stars. We find that the errors require correction on the order of 20%, and that without this correction even non-variable standard stars show structure function variability on the level of 0.1 mag. Through analysis of χ distribution we show that the listed errors are under- or overestimated.
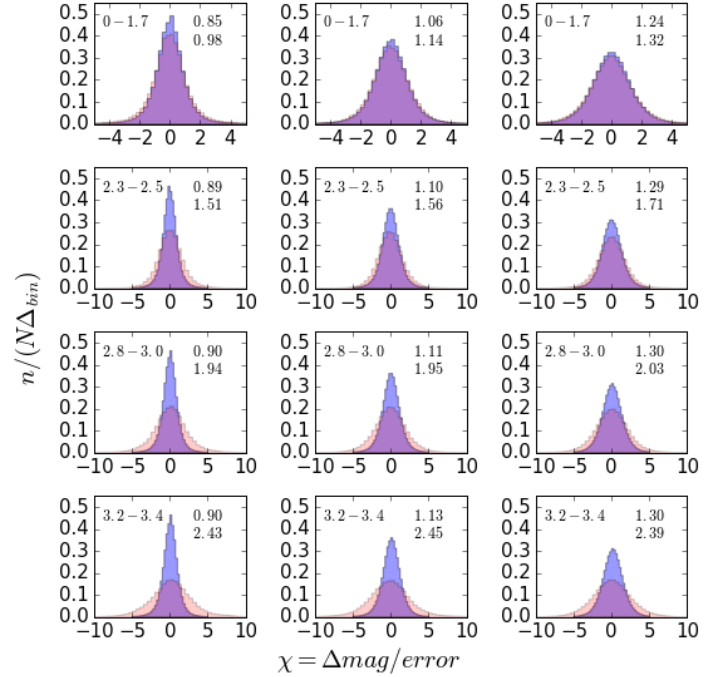
Figure 3. This grid of histograms shows $\chi = \Delta m$/error for CRTS blue stars (blue shading) and quasars (red shading), for bins of $\log \Delta t$- SDSS r magnitude. Vertically, from top to bottom, we iterate over bins of $\log \Delta t$: $0 < \log \Delta t < 1.7$ ($t < 50$ days) ,$2.3 < \log \Delta t < 2.5$, $2.8 < \log \Delta t < 3.0$, and $3.2 < \log \Delta t < 3.4$ (indicated by numbers in the upper left corner of each subplot). Horizontally, from left to right, we iterate over SDSS r-magnitude bins $17-18$, $18-18.5$, and $18.5-19$. Objects in each vertical strip were chosen according to the same magnitude cut, and all Δm points in a given $\log \Delta t$ range were binned together. The implied small quasar variability at short timescales is at the level measured by SDSS (indistinguishable from blue, non-variable stars). Numbers in the upper-right corner of each subplot are the robust width of stellar and quasar distributions of χ. Blue, bright stars in the left strip ($17-18$ r mag) have low σ_G, at the level of 0.9, and fainter blue stars (eg. right vertical strip, $18.5-19$ r mag) have higher $\sigma_G \approx 1.3$. Part of that increase is due to larger errors at fainter magnitude end. However, in each bin we expect that if errors for blue stars are correct, then $\sigma_G(\chi) = 1$. We use correction factors $f_c = \sigma_G(\chi_{blue}(\Delta t, mag))$ to correct for that effect. This implies that magnitude-difference errors $\sigma_{corr}(\Delta m) = f_c\sigma(\Delta m)$. If all raw errors were identical, it would also correspond to the linear correction of raw photometric errors by f_c. Quasars as intrinsically variable sources have a larger spread of χ than non-variable blue stars, but after applying the f_c correction their short-timescale χ at $t < 50$ days becomes much closer to 1, consistent with lack of variability (see Fig.4 for an illustration of the impact of f_c on SF of stars and quasars).
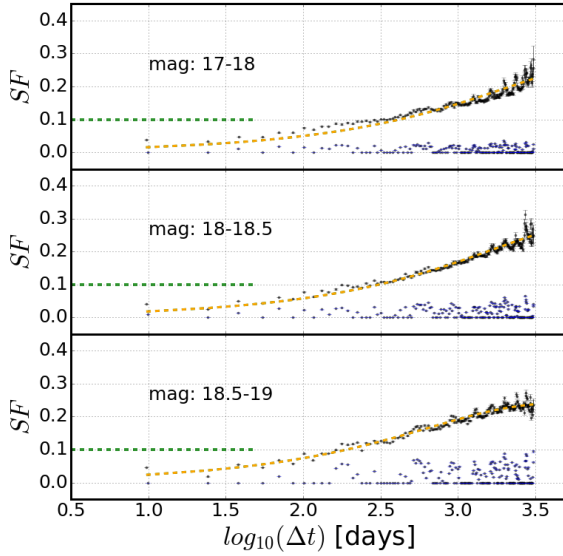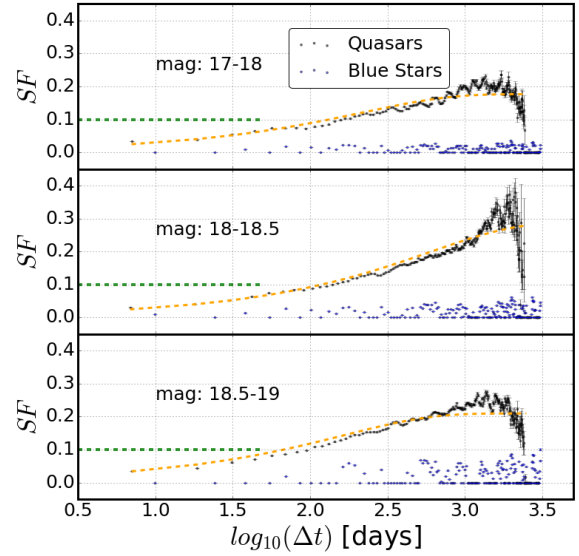
Figure 4. Three panels depict the impact that applying correction factors $f_c(\Delta t, mag)$ to errors $\sigma(\Delta m)$ has on the structure function (σ) for quasars and blue stars. In the middle of each panel we list the SDSS r-magnitude used to select quasars and stars for that magnitude bin. Note that with f_c the apparently discrepant variability of non-variable standard stars vanishes (the residual SF is consistent with the noise rms of 0.05 mag). The variability of quasars is reduced . We plot the observed frame timelags - see Fig.5 for the effect of converting that to the restframe timelags using known quasar redshifts from SDSS. The corrected SF of quasars at short time scales ($\log(\Delta t) < 1.7$) is consistent with lack of variability, consistent with SDSS results (upper limits of 0.1 mag marked by green dashed lines) (see (MacLeod et al. 2011)).

Figure 5. Three panels depict the impact that applying correction factors $f_c(\Delta t, mag)$ to errors $\sigma(\Delta m)$ has on the structure function (σ) for quasars and blue stars in the quasar restframe. In the middle of each panel we list the SDSS r-magnitude used to select quasars and stars for that magnitude bin. We plot the rest frame timelags, with $t_{rest} = t_{obs}/(1 + z)$ (MacLeod et al. 2010) . This shifts time lags to shorter timescales, but does not affect our predictions about the lack of variability in quasars on short timescales ($\log(\Delta t) < 1.7$). The apparent downturn in the SF of quasars, as compared to Fig.4, is due to smaller number of points in bins of higher Δt due to redshift correction, which leads to smaller bin dispersion in Δm.

APPENDIX A

In Sec. 4 we show how f_c corrects the value of the magnitude-difference error : $\sigma_{j,k}(\Delta m_{j,k})$. Now since $\sigma_j(m_j) = 1/\sqrt{\sum w_j}$, and $w_j = 1/e_j^2$, if we assume that errors are homoscedastic, i.e. $e_j = e$, then $\sigma(m) = e/\sqrt{M}$, where M is the number of intra-night observations. So since we require $\sigma(\Delta m)_{NEW} = f_c \sigma(\Delta m)_{OLD}$, we have $e_{NEW} = f_c e_{OLD}$, i.e. f_c applies as a multiplicative correction factor both for weight-based day-averaged magnitude errors, as well as the raw errors.

REFERENCES

Abazajian, K. N., et al. 2009, ApJS, 182, 543

Astropy Collaboration, et al. 2013, A&A, 558, A33

Charisi, M., Bartos, I., Haiman, Z., Price-Whelan, A. M., Graham, M. J., Bellm, E. C., Laher, R. R., & Márka, S. 2016, MNRAS, 463, 2145

Collier, S., & Peterson, B. M. 2001, ApJ, 555, 775

de Vries, W. H., Becker, R. H., White, R. L., & Loomis, C. 2005, AJ, 129, 615

Djorgovski, S. G., et al. 2011, ArXiv e-prints

Drake, A. J., et al. 2013, ApJ, 763, 32

Graham, M. J., Djorgovski, S. G., Drake, A. J., Mahabal, A. A., Chang, M., Stern, D., Donalek, C., & Glikman, E. 2014, MNRAS, 439, 703

Graham, M. J., et al. 2015, MNRAS, 453, 1562

Graham, M. J., Drake, A. J., Djorgovski, S. G., Mahabal, A. A., Donalek, C., Duan, V., & Maker, A. 2013, MNRAS, 434, 3423

Hawkins, M. R. S. 2002, MNRAS, 329, 76

Ivezić, Ž., Connelly, A. J., VanderPlas, J. T., & Gray, A. 2014, Statistics, Data Mining, and Machine Learningin Astronomy

Ivezić, Ž., et al. 2007, AJ, 134, 973

Kawaguchi, T., Mineshige, S., Umemura, M., & Turner, E. L. 1998, ApJ, 504, 671

Kelly, B. C., Bechtold, J., & Siemiginowska, A. 2009, The Astrophysical Journal, 698, 895

Kelly, B. C., Bechtold, J., Siemiginowska, A., Aldcroft, T., & Sobolewska, M. 2007, ApJ, 657, 116

Kelly, B. C., Sobolewska, M., & Siemiginowska, A. 2011, ApJ,

730, 52

Kozłowski, S. 2016, ApJ, 826, 118

Lawrence, A. 2016, in Astronomical Society of the Pacific Conference Series, Vol. 505, Astronomical Surveys and Big Data, ed. A. Mickaelian, A. Lawrence, & T. Magakian, 107

MacLeod, C. L., et al. 2011, The Astrophysical Journal, 728, 26

MacLeod, C. L., et al. 2010, The Astrophysical Journal, 721, 1014

Schmidt, K. B., Marshall, P. J., Rix, H.-W., Jester, S., Hennawi, J. F., & Dobler, G. 2010, ApJ, 714, 1194

Schneider, D. P., et al. 2008, VizieR Online Data Catalog, 7252

Sesar, B., et al. 2007, The Astronomical Journal, 134, 2236

Süveges, M., et al. 2012, MNRAS, 424, 2528

Vanden Berk, D. E., et al. 2004, ApJ, 601, 692

Zu, Y., Kochanek, C. S., Kozłowski, S., & Udalski, A. 2013, ApJ, 765, 106

This paper has been typeset from a TeX/LaTeX file prepared by the author.